

# RSC Applied Interfaces

Accepted Manuscript

This article can be cited before page numbers have been issued, to do this please use: R. Tan, E. Thomas, N. Marzolini and Y. Jang, *RSC Appl. Interfaces*, 2026, DOI: 10.1039/D6LF00023A.



This is an Accepted Manuscript, which has been through the Royal Society of Chemistry peer review process and has been accepted for publication.

Accepted Manuscripts are published online shortly after acceptance, before technical editing, formatting and proof reading. Using this free service, authors can make their results available to the community, in citable form, before we publish the edited article. We will replace this Accepted Manuscript with the edited and formatted Advance Article as soon as it is available.

You can find more information about Accepted Manuscripts in the [Information for Authors](#).

Please note that technical editing may introduce minor changes to the text and/or graphics, which may alter content. The journal's standard [Terms & Conditions](#) and the [Ethical guidelines](#) still apply. In no event shall the Royal Society of Chemistry be held responsible for any errors or omissions in this Accepted Manuscript or any consequences arising from the use of any information it contains.

1  
2  
3  
4  
5  
6  
7  
8  
9  
10  
11  
12  
13  
14  
15  
16  
17  
18

# Stiffness-Driven Modulation of Bactericidal Behavior in Nanostructured Polymer Thin Films

*Ruwen Tan,<sup>+</sup> Emma Thomas,<sup>+</sup> Nicolas Marzolini, Yeongseon Jang\**

*Department of Chemical Engineering, University of Florida, Gainesville, FL, 32611, USA*

<sup>+</sup> Co-first authors

\*Corresponding author

KEYWORDS: Bactericidal Nanostructure, *Escherichia coli*, *Staphylococcus aureus*, Polymer Thin Films, Mechanical Properties, Nanotechnology.



## 1 ABSTRACT

2 The increasing use of medical implants, coupled with rising antimicrobial resistance, has  
3 intensified the need for effective antibacterial surface technologies. Protrusive nanostructured  
4 surfaces can mechanically disrupt bacterial membranes, leading to cell death, and have inspired  
5 extensive biomimetic design strategies. While prior studies have focused on the roles of  
6 nanostructure geometry, density, and surface chemistry, the intrinsic stiffness of nanostructured  
7 surfaces retaining the same structures and chemistry remains not fully understood. Here, we  
8 systematically investigate the relationship between nanostructure stiffness and bactericidal  
9 efficacy by fabricating nanostructured polymer surfaces with tunable Young's moduli. Using  
10 *Escherichia coli* and *Staphylococcus aureus* as model Gram-negative and Gram-positive bacteria,  
11 respectively, we demonstrate that bactericidal efficacy against *E. coli* decreases with reduced  
12 nanostructure stiffness, consistent with diminished membrane tension. In contrast, *S. aureus*  
13 exhibits lower sensitivity to stiffness changes at higher moduli, reflecting its thicker and  
14 mechanically robust cell envelope. Notably, the softest nanopillars yield the highest bactericidal  
15 efficacy against *S. aureus*, attributed to enhanced nanopillar–cell interactions arising from bacterial  
16 cell geometry and increased structural deformability. Furthermore, highly deformable  
17 nanostructures promote additional bactericidal effects through lateral squeezing and cell sinking  
18 mechanisms. These findings reveal that bacterial cell size and morphology, in conjunction with  
19 nanostructure stiffness, critically govern bactericidal performance. This work provides  
20 mechanistic insight into stiffness-mediated bacterial membrane disruption and offers design  
21 principles for optimizing next-generation antibacterial surfaces.



## 1 INTRODUCTION

2 The development of antibacterial surfaces is increasingly important for mitigating  
3 microbial contamination in medical and industrial settings.<sup>1-3</sup> Traditional approaches rely on  
4 bacterial-repelling antifouling coatings<sup>4</sup> or bacterial-killing strategies using biocidal agents.<sup>5, 6</sup>  
5 However, these strategies are often limited by reduced long-term efficacy, potential toxicity, and  
6 the emergence of antimicrobial resistance.<sup>7-11</sup> As an alternative, nanostructured surfaces that  
7 physically disrupt bacterial membranes have emerged as a promising non-chemical strategy for  
8 bacterial inactivation. Bioinspired nanostructures, such as those found on cicada and dragonfly  
9 wings, have demonstrated the ability to mechanically disrupt bacterial membranes<sup>12, 13</sup> These  
10 studies established that bactericidal activity arises primarily from physical interactions rather than  
11 surface chemistry, motivating the development of artificial nanostructured, bactericidal surfaces  
12 with controlled geometry.<sup>14-16</sup>

13 A wide range of nanostructured materials, including silica,<sup>17</sup> titanium,<sup>18, 19</sup> stainless steel,<sup>20</sup>  
14 aluminum,<sup>21</sup> copper,<sup>21</sup> gold,<sup>22</sup> and polymer,<sup>23</sup> have showed bactericidal efficacy, reinforcing the  
15 hypothesis that the mechanical interactions between surface nanostructures and adhered bacteria  
16 dominate over surface chemistry effects. Previous studies have shown that nanopillar geometry,  
17 including height, diameter, and spacing (density), strongly influences bacterial performance.<sup>1, 10,</sup>  
18 <sup>17, 24-27</sup> Reported bactericidal nanopillars typically fall within ranges of 100–900 nm in height, 20–  
19 207 nm in diameter, and 9–380 nm in interpillar spacing.<sup>25</sup>

20 Bacterial properties, including cell size, membrane rigidity, and surface-associated  
21 biomolecules, also influence survival on nanostructured surfaces.<sup>24, 28</sup> For instance, Gram-negative  
22 bacteria such as *P. aeruginosa* are readily damaged by bioinspired nanopillars, whereas Gram-  
23 positive bacteria with thicker and mechanically robust cell envelopes (e.g., *B. subtilis*, *P. maritimus*,



1 *and S. aureus*) often remain intact under similar conditions.<sup>13, 29</sup> These observations indicate that  
2 bacterial membrane rigidity is a key determinant of resistance to mechanical disruption. Given that  
3 bactericidal activity arises from physical interactions between the cell and nanostructure, we  
4 hypothesize that nanostructure stiffness, analogous to bacterial shape and rigidity, also plays a  
5 critical role in governing bactericidal efficacy.

6 While geometric parameters have been extensively studied for bactericidal performance  
7 across various bacterial types, the role of nanostructure stiffness and its coupling with bacterial  
8 cell mechanics remains insufficiently understood. In most prior work, nanostructures are fabricated  
9 from rigid inorganic materials (e.g., metals,<sup>18, 20-22</sup> silicon (Si),<sup>14, 26, 30</sup> and silicon oxide<sup>17</sup>), where  
10 deformation during bacterial adhesion is minimal.<sup>31, 32</sup> In these systems, stiffness has typically  
11 been varied by altering nanopillar geometry,<sup>17, 26, 27</sup> making it difficult to decouple mechanical  
12 effects from structural parameters and leading to inconsistent observations across studies.<sup>33 34, 35</sup>  
13 Furthermore, while rigid inorganic nanostructures often exhibit strong bactericidal efficacy, they  
14 offer limited tunability and are not well suited for applications requiring flexibility,  
15 biocompatibility, or scalable processing. In contrast, in more compliant systems, nanopillars can  
16 undergo bending or deformation upon bacterial adhesion,<sup>26, 36, 37</sup> potentially altering cell-surface  
17 interactions and bactericidal outcomes.

18 Poly(ethylene glycol) dimethacrylate (PEGDMA) is a promising material platform due to  
19 its antifouling characteristics, biocompatibility, and ability to form well-defined nanostructures.<sup>36,</sup>  
20 <sup>38-40</sup> Prior studies have explored PEGDMA-based systems in related contexts: Kim *et al.*  
21 demonstrated that PEGDMA nanopillars possess sufficient stiffness to deform bacteria upon  
22 attachment but did not investigate stiffness-dependent bactericidal efficacy.<sup>38</sup> Kolewe *et al.*  
23 reported that PEGDMA stiffness influences bacterial adhesion on flat surfaces without



1 incorporating nanostructures.<sup>41</sup> Together, these studies highlight the need to systematically  
2 investigate stiffness effects in nanostructured polymer systems.

3 To address this gap, we investigate the effect of nanostructure stiffness on bactericidal  
4 efficacy while maintaining consistent surface topography. Specifically, we tune the effective  
5 stiffness of nanopillars by varying the Young's modulus of PEGDMA networks with different  
6 crosslinking densities. Although this approach enables systematic control of stiffness, we note that  
7 changes in polymer modulus may also influence hydration and viscoelasticity, which could  
8 contribute to bacterial-surface interactions.<sup>42</sup> While these coupled effects cannot be fully  
9 decoupled, the use of colloidal lithography and soft molding to maintain consistent nanostructure  
10 geometry provides a controlled framework to examine its influence on bactericidal behavior.<sup>43</sup>  
11 When compared to other nanopatterning methods, such as photolithography<sup>44</sup>, electron beam  
12 lithography<sup>45</sup>, focused ion beam lithography<sup>46</sup>, soft lithography<sup>47</sup>, and nanoimprinting<sup>48</sup>, colloidal  
13 lithography offers low costs, high throughput, and accessibility.<sup>49</sup>

14 Herein, using nanostructured PEGDMA thin films with controlled nanoscale geometry, we  
15 evaluate bactericidal performance against a representative Gram-negative bacterium, *E. coli* K12,  
16 and a Gram-positive bacterium, Methicillin-resistant *Staphylococcus aureus* (MRSA). We further  
17 examine the role of externally applied forces by introducing surface-tension-driven loading during  
18 drying. This study provides insights into how nanostructure stiffness and bacterial cell properties  
19 collectively influence bactericidal behavior and offers design considerations for mechanically  
20 tunable antibacterial surfaces.



## 1 EXPERIMENTAL SECTION

2       **Materials:** Silicon (Si) wafers (4-inch, P-type, <100>), purchased from University Wafer  
3 Inc., were used as a substrate to make a master mold. Silica (SiO<sub>2</sub>) particles with diameters of ~350  
4 nm (Particle Solutions LLC), serving as masks in colloidal lithography, were prepared by a  
5 modified Stöber method.<sup>50</sup> Ethanol (Reagent Alcohol) used to clean particles was purchased from  
6 Fisher Chemical. Perfluoropolyether (PFPE, Fluorolink MD700, Solvay) was used as a soft mold  
7 for pattern transfer. Poly (ethylene glycol) dimethacrylate (PEGDMA, M<sub>n</sub> ~ 350, Polysciences  
8 Inc., M<sub>n</sub> ~ 550 and 750, Sigma Aldrich) and Darocur 1173 (photoinitiator, Sigma Aldrich) were  
9 used to obtain positive patterns from the Si master mold via soft mold pattern transfer upon  
10 ultraviolet (UV) irradiation. Lysogeny broth (LB) and Tryptic Soy Broth (TSB), purchased from  
11 Fisher BioReagents and BD Bacto, were used to make LB media and TSB media for bacterial  
12 culture.

13       **Measurement of Mechanical Properties by Micro-indentation:** Micro-indentation was  
14 performed by following the protocol described in a previous work.<sup>51</sup> Briefly, the flat polymer  
15 hydrogel films were placed on the stage and indented with a piezo-driven, quasistatic transducer  
16 indentation system (Hysitron BioSoft) with a hemispherical indenter tip. The indentation tip, a  
17 borosilicate glass hemisphere with a radius of 1 mm, indented the polymer thin films in the air (or  
18 in MilliQ water) at a constant piezo displacement rate of 250 nm/s in a displacement-controlled  
19 operation mode at 5 random points. Force-response and positions were measured simultaneously  
20 by the quasistatic transducer at a rate of 125 Hz. The Young's modulus and other mechanical  
21 properties were calculated by analyzing the force-displacement curve with MATLAB.

22       **Colloid Lithography to Create Nanopillars on Silicon (Si) Master Mold:**  
23 Monodispersed colloidal SiO<sub>2</sub> microspheres with diameters of 350 nm were cleaned by repeating



1 5 cycles of centrifugation and redispersion in ethanol. A monolayer of close-packed SiO<sub>2</sub> particle  
2 array was coated on a 4-inch Si wafer by Langmuir-Blodgett coating.<sup>52</sup> Briefly, the wafer was  
3 vertically pulled up by a syringe pump at a speed of 5 mm/min from water, while the SiO<sub>2</sub> particles,  
4 dispersed in ethylene glycol (Alfa Aesar, 99 %) with a volume fraction of 1 %, were added on the  
5 water/air interface. The close-packed SiO<sub>2</sub> arrays served as masks during reactive ion etching (RIE,  
6 Unaxis Shuttlelock Reactive Ion Etcher) using an SF<sub>6</sub>/O<sub>2</sub> gas mixture (5 mTorr, 20 SCCM SF<sub>6</sub>,  
7 20 SCCM O<sub>2</sub>, 150W, for 4 min) to fabricate Si nanopillars beneath.<sup>53</sup> The SiO<sub>2</sub> particles were  
8 finally removed by immersing the etched wafer in a 2 vol % hydrofluoric acid aqueous solution  
9 for 2 min.

10 **Fabrication of Nanostructure on Polymer Thin Films:** Si master mold with nanopillars  
11 was treated with trichloro-(1H, 1H, 2H, 2H-perfluorooctyl) silane (Sigma Aldrich) to lower the  
12 surface energy. A soft negative mold with the inverted pattern of the Si master mold was fabricated  
13 by drop-casting PFPE mixed with 4 wt % photoinitiator, followed by UV-induced polymerization  
14 at a wavelength of 365 nm for 15 min under N<sub>2</sub>.<sup>54</sup> Using the PFPE soft negative mold, the  
15 nanopillar pattern was transferred from the Si master mold to the target polymer thin films. A drop  
16 of the PEGDMA oligomer solution containing 0.4 wt % photoinitiator was placed between a PFPE  
17 soft mold and a glass slide. Crosslinked PEGDMA thin films with nanopillars were easily peeled  
18 off from the PFPE soft molds after 15 min of UV exposure.

19 **Bacterial Cell Culture and Bacterial Live/Dead Assay:** *E. coli* K12 KCJ140 (or *S.*  
20 *aureus* MRSA KCJ3K555) was pre-cultured in 5 mL of LB (or TSB) media overnight. 50 μL of  
21 the pre-cultured bacterial solution was transferred to 5 mL fresh LB media (or TSB media) for an  
22 additional incubation in a shaking incubator until late log (optical density at 600 nm, OD<sub>600</sub>=1.0)  
23 phase. 1 mL of the diluted bacterial solution with OD<sub>600</sub>=0.1 (~10<sup>7</sup> cells/mL) in phosphate-buffered



1 saline (PBS) was added to each well of a 24-well plate containing samples. Then, the samples were  
2 incubated at 37 °C for 1 h and 4 h. At the end of incubation, each sample was gently rinsed twice  
3 with 1 mL PBS to remove non-attached bacteria. To evaluate the viability of bacteria adhered in  
4 the wet condition, the samples were stained with a Live/Dead BacLight bacterial viability kit  
5 (L7012, Life Technologies) according to the manufacturer's protocol. Briefly, 1.5  $\mu$ L of 3.34 mM  
6 SYTO9 (stain live cells with intact membranes with green fluorescent color) and 1.5  $\mu$ L of 20 mM  
7 propidium iodide (stain dead cells with damaged membranes with red fluorescent color) were  
8 mixed in 1 mL of PBS. Each sample was immersed in the staining solution individually and  
9 incubated in the dark for 15 min. The samples were transferred to a glass slide, covered with a  
10 cover slip to prevent water evaporation. Then, the samples were imaged using a fluorescent  
11 microscope (Zeiss, AxioObserver7) equipped with a 20 $\times$  objective lens. To further evaluate the  
12 effect of the nanostructure's mechanical properties on the surface-tension-driven bactericidal  
13 efficacy, the samples incubated for 4 h were treated with a sequential short-time drying step,  
14 following a protocol from previous work.<sup>55</sup> Briefly, the nanostructured samples were incubated in  
15 bacterial solution for 4 h and washed with PBS as previously described. Then, the samples were  
16 sequentially dried in air for 60 s by allowing the water thin film on the surface to evaporate. The  
17 samples were then stained and imaged with the same procedure described above. Images were  
18 taken at 5 random points on each sample, and the number of bacteria on each image was analyzed  
19 by the image-based tool for counting nuclei (ITCN) plugin in ImageJ. The statistical analysis of  
20 bacterial adhesion and viability was performed using a One-way ANOVA in GraphPad.

21 **Scanning electron microscopy (SEM) for monitoring morphologies of nanostructured**  
22 **surfaces and adhered bacteria:** To visualize the morphology of the nanostructure on the surfaces  
23 and adhered bacteria by SEM, samples were prepared and incubated in bacterial solution with the



1 same procedure described above. After 4 h incubation, samples were gently washed with 1 mL  
2 PBS twice, fixed in 2.5 % glutaraldehyde (TCI America) solution for 1 h at 4 °C, and dehydrated  
3 using a series of ethanol concentrations in distilled water (i.e., 50, 70, 90, and 100 % for 20 min,  
4 respectively). The dehydrated samples were further dried with hexamethyldisilazane (HDMS, Alfa  
5 Aesar, 98 %) overnight. To visualize the morphology of the nanostructure on the surfaces and  
6 adhered bacteria after air-drying for 60 s while minimizing the introduction of additional surface  
7 tension, the dried samples were fixed in 2.5 % glutaraldehyde and freeze-dried in a lyophilizer  
8 (Labconco, FreeZone 2.5 Plus) overnight to ensure complete dehydration. The prepared samples  
9 were then sputtered with gold (10 nm). Bacterial morphology was characterized using SEM (FEI  
10 Nova NanoSEM 430) at an acceleration potential of 3 kV.

11 **Statistical Analysis:** All quantitative data are reported as mean  $\pm$  standard error of the  
12 mean (SEM). For each sample condition, fluorescence images were collected from five randomly  
13 selected locations per sample, and bacterial counts were obtained using the ImageJ ITCN plugin  
14 as described above. Statistical analysis of bacterial adhesion and viability between different sample  
15 groups was performed using one-way analysis of variance (ANOVA) in GraphPad. Statistical  
16 significance between groups was evaluated using the following thresholds: \*\*ns (not significant),  
17  $p > 0.05$ ; \* $p < 0.05$ ; \*\* $p < 0.01$ ; \*\*\* $p < 0.001$ ; \*\* $p < 0.0001$ .

18



## 1 RESULTS AND DISCUSSION

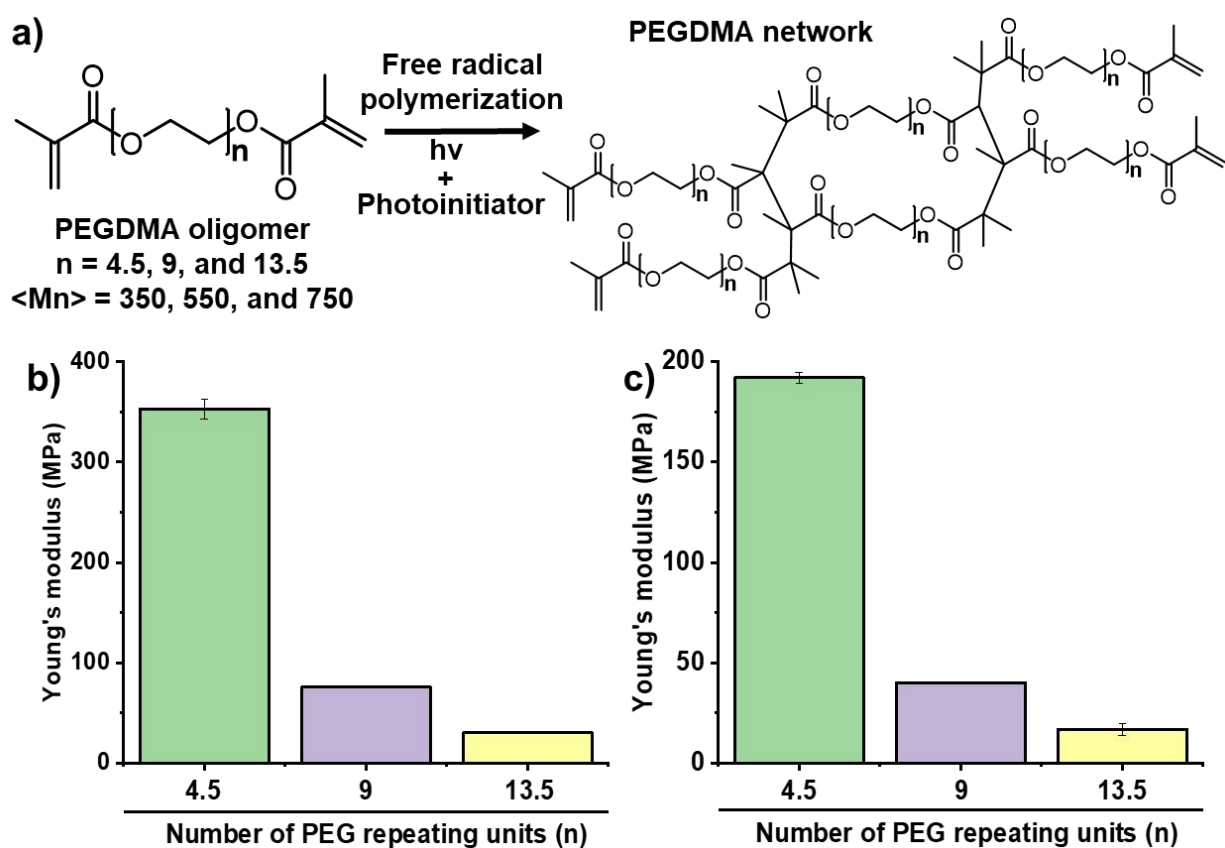
### 2 Tuning Young's Moduli of Polymer Thin Films.

3 Poly(ethylene glycol) dimethacrylate (PEGDMA), a biocompatible polymer with moderate  
4 tunability of its properties, has been widely used as the major or added component in polymers for  
5 many bio-applications, such as bone generation and tissue scaffolding.<sup>56-58</sup> Here, we tailored the  
6 Young's moduli of network polymer thin films by changing their crosslinking density through  
7 polymerization of the PEGDMA oligomers with different average PEG repeating units ( $n$ ) of 4.5,  
8 9, and 13.5. **Figure 1a** shows the free radical polymerization of PEGDMA oligomers into the  
9 networks in the presence of photoinitiator and UV exposure. PEGDMA thin films with 4.5 PEG  
10 repeating units showed the highest Young's modulus, 353 MPa in air, while the Young's modulus  
11 decreased to 75 MPa and 30 MPa in air when  $n$  was increased to 9 and 13.5, respectively (**Figure**  
12 **1b**). The Young's modulus was measured from PEGDMA thin films and used as an estimate of  
13 the effective material modulus governing nanopillar behavior, recognizing that geometric  
14 confinement and nanoscale effects may lead to deviations from bulk values. It should also be noted  
15 that variations in crosslinking density may influence polymer hydration and viscoelastic  
16 properties, in addition to stiffness.<sup>59</sup>

17 The polymerization of PEGDMA oligomers with fewer PEG repeating units leads to higher  
18 crosslinking densities in the polymer networks, resulting in higher Young's moduli.<sup>60</sup> Because the  
19 antibacterial performances of polymer samples are evaluated in aqueous solution, we further  
20 assessed the Young's moduli of PEGDMA thin films that were swollen in water for 24 hours  
21 (**Figure 1c**). The fully swollen PEGDMA thin films also showed a reduction in Young's modulus  
22 as their crosslinking densities decreased. The absorption of water molecules on the PEG chains  
23 reduces the crosslinking concentration and Young's modulus compared with their moduli in air.<sup>60</sup>



1 As a result, we tailored the Young's moduli of PEGDMA thin films made from oligomers  
 2 containing an average of 4.5, 9, and 13.5 PEG repeating units to 190 MPa, 40 MPa, and 17 MPa  
 3 in water, respectively. Prior studies on PEGDMA hydrogels typically report moduli in the kPa  
 4 range and modulate stiffness through polymer weight fraction, with a primary focus on bacterial  
 5 adhesion.<sup>41, 61, 62</sup> In contrast, the present work investigates PEGDMA thin films with substantially  
 6 higher moduli in the MPa range and evaluates both bactericidal efficacy and adhesion. Notably,  
 7 while previous studies have largely examined flat hydrogel substrates, our approach integrates  
 8 stiffness control within nanostructured architectures.



10  
 11 **Figure 1.** a) PEGDMA oligomers containing an average of 4.5, 9, and 13.5 PEG repeating units  
 12 are polymerized into flat PEGDMA networks in the presence of photoinitiator and UV exposure.



1 b-c) Young's moduli of PEGDMA thin films measured by micro-indentor in air (b) and in water  
2 (c).

#### 4 **Fabricating Nanopillars on PEGDMA Thin Films.**

5 The nanopillar geometry used in this study (average spacing  $\sim 350$  nm, height  $\sim 500$  nm, tip  
6 diameter  $\sim 110$  nm, and base diameter  $\sim 230$  nm) was selected based on our prior work, optimizing  
7 nanopatterned polymer surfaces for maximal bactericidal efficacy.<sup>26</sup> While previous studies from  
8 our group compared flat and nanostructured surfaces across varying densities, the present work  
9 maintains this optimized geometry and focuses specifically on isolating the effect of stiffness.  
10 **Figure 2a** shows the schematics of fabricating bactericidal nanopillars on the Si and transferring  
11 them to PEGDMA thin films. Colloidal lithography using monodispersed SiO<sub>2</sub> nanoparticles as  
12 etching masks and SF<sub>6</sub>/O<sub>2</sub> as etching gas enables the creation of ordered, uniform nanopillars  
13 across the entire Si master, providing an ideal platform to study the effect of nanopillar stiffness  
14 while minimizing the influence of surface topography variation.<sup>52, 53</sup> A soft molding pattern  
15 transfer was then used to replicate the nanopillars from the Si master to target PEGDMA thin films.  
16 In the procedures, the perfluoropolyether (PFPE), a fluoro-polymer with low shrinkage upon  
17 polymerization and low surface energy, allows the precise replication of inverted structures on the  
18 negative mold.

19



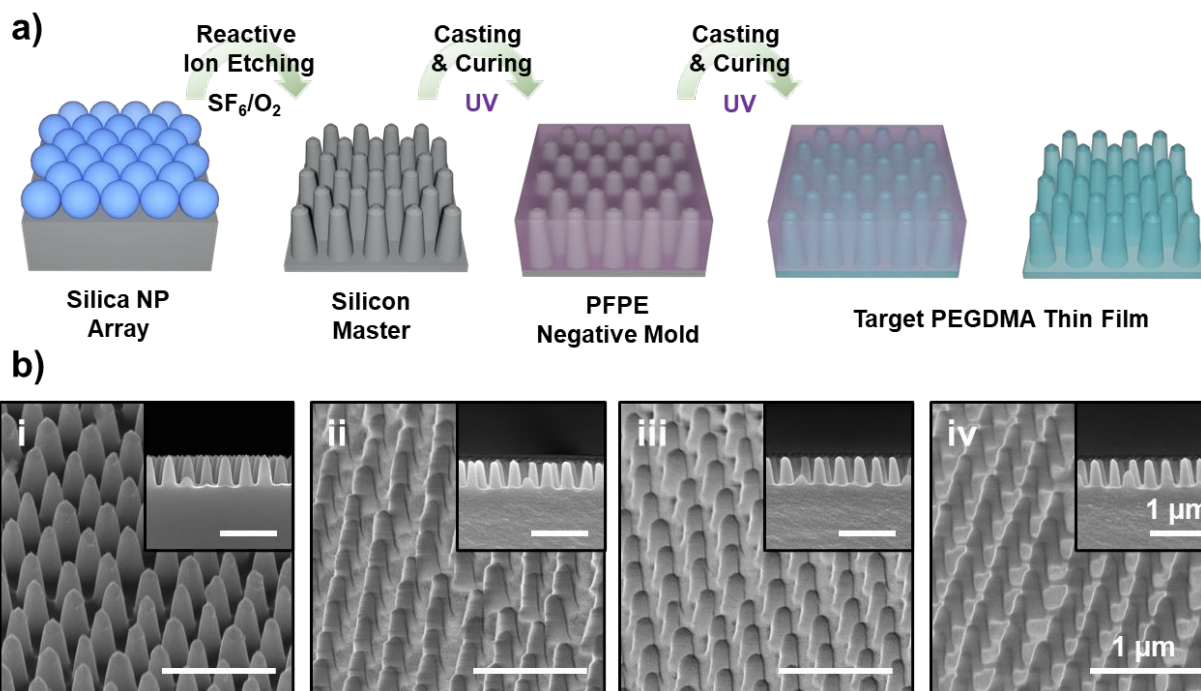


**Figure 2.** a) Schematic illustration of the fabrication of nanopillars on PEGDMA thin films by colloidal lithography using  $\text{SiO}_2$  nanoparticles and soft molding pattern transfer using PFPE. b) Tilted-view SEM images of the nanopillars fabricated on i) Si and PEGDMA thin films polymerized from oligomers with PEG repeating units ( $n$ ) of ii) 4.5, ii) 9, and iii) 13.5. The inset images represent the cross-sectional views of the samples. All scale bars are  $1 \mu\text{m}$ .

Eventually, the nanopillars with different Young's moduli were fabricated on the target PEGDMA thin films by casting and curing their oligomers on the negative mold. **Figure 2b** shows scanning electron microscopy (SEM) images of the nanopillars fabricated on the Si master and PEGDMA thin films. The nanopillars fabricated on the PEGDMA thin films shared similar geometric parameters but differed in Young's modulus, enabling investigation of nanopillar stiffness and its impact on bactericidal efficacy. The detailed geometric parameters of



1 nanostructured Si and nanostructured PEGDMA thin films are summarized in **Table S1 in the**  
2 **Supporting Information.**

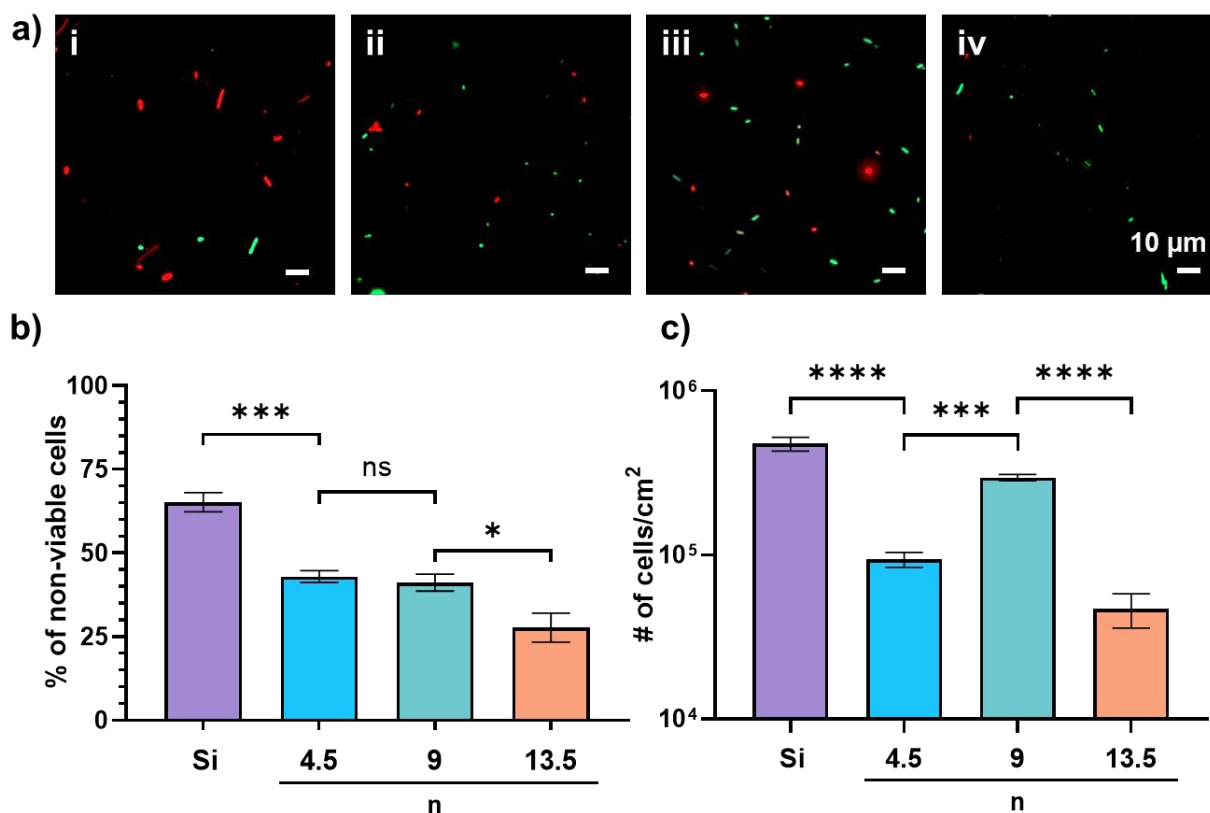
3  
4 **Understanding the Relationship between Nanopillar Stiffness and the Bactericidal Efficacy**  
5 **against *E. coli*.**

6 A model Gram-negative bacterium, *E. coli* K12, which is a completely genome sequenced  
7 bacterium and widely used for assessing bactericidal efficacy,<sup>63, 64</sup> was used to evaluate the effect  
8 of nanopillar stiffness on antibacterial performance. We performed bacterial live/dead assays  
9 (**Figure 3a**) by observing the fluorescent signals of adhered bacteria on nanopillars after 4 h  
10 incubation in bacterial solution, allowing for sufficient bacterial adhesion.<sup>26</sup> In this assay, SYTO  
11 9 can penetrate into the live cells with intact membranes and stain nucleic acids a fluorescent green,  
12 whereas propidium iodide only diffuses into cells with damaged membranes and stains the nucleic  
13 acid of non-viable cells a fluorescent red.<sup>65</sup> The percent of non-viable cells was calculated by  
14 dividing the number of non-viable red cells by the total number of cells adhered to the area of  
15 interest (**Figure 3b**). We evaluated the bactericidal efficacy by the percentage of non-viable cells  
16 among the total bacteria adhered. The bactericidal nanopillars fabricated on Si with a Young's  
17 modulus of 169 GPa were used as the control due to their sufficient stiffness and well-known  
18 bactericidal efficacy against *E. coli*.<sup>14, 31</sup> Importantly, these Si nanopillars represent an upper bound  
19 in stiffness, enabling benchmarking of polymer-based nanostructures and isolating the role of  
20 mechanical compliance on bactericidal performance.

21 After *E. coli* incubation with the samples for 4 hours, we confirmed that 66 % of adhered  
22 *E. coli* cells were dead on hard Si nanopillars, while the percentage of non-viable cells on the  
23 PEGDMA nanopillars decreased from 43 % to 28 % as the surfaces' elastic moduli decreased from



1 190 MPa to 17 MPa. We also confirmed that the highest total number of adhered bacteria was  
 2 observed on Si nanopillars, whereas reduced bacterial adhesion was observed on PEGDMA  
 3 nanopillars, with variation among surfaces (**Figure 3c**). The adhesion density of *E. coli* on  
 4 PEGDMA nanopillars ranged from  $10^4$  to  $10^5$  cells per square centimeter across all Young's  
 5 moduli. Interestingly, the highest adhesion of *E. coli* was observed on nanopillars of intermediate  
 6 stiffness ( $n = 9$ ). Bacterial adhesion is influenced by multiple factors, including surface topography,  
 7 wettability, stiffness, and charge.<sup>66</sup> The enhanced adhesion at intermediate stiffness may reflect a  
 8 balance between structural compliance and mechanical support, where sufficient deformation  
 9 increases bacteria–surface contact area while maintaining stable anchoring points. However, this  
 10 interpretation remains qualitative.



11



1 **Figure 3.** a) Representative fluorescent microscopic images of *E. coli* K12 on nanopillars of i) Si,  
2 PEGDMA with n of ii) 4.5, iii) 9, and iv) 13.5 after 4 h cultivation in a static incubator at 37 °C.  
3 All scale bars are 10 μm. b) Quantitative image analysis on the percentage (%) of non-viable cells  
4 attached to the samples after 4 h of cultivation. c) Quantitative image analysis of the number of  
5 cells attached to the samples after 4 h of cultivation. (Data represent mean ± SEM. ns (not  
6 significant):  $p > 0.05$ ; \* $p < 0.05$ , \*\* $p < 0.01$ , \*\*\* $p < 0.001$ , \*\* $p < 0.0001$ )  
7

8 The dependence of bactericidal efficacy on the surface nanostructure stiffness can be  
9 modeled by a biophysical framework describing the different cell-nanopillar interactions under the  
10 driving force of the interfacial energy gradient. Three interfaces of bacterium-liquid, bacterium-  
11 solid, and solid-liquid exist when a bacterium attaches to a nanostructured surface. The total  
12 interfacial energy of the system is determined by the summation of individual interface/surface  
13 energies ( $\sigma$  or  $\gamma$ ) between the bacterium-liquid ( $A_{BL}\sigma_{BL}$ ), bacterium-solid ( $A_{BS}\sigma_{BS}$ ), and solid-  
14 liquid ( $A_{SL}\gamma_{SL}$ ) at given contact areas ( $A$ ).<sup>67</sup> The total interfacial energy decreases as the contact  
15 area between a bacterial membrane and the nanostructure increases, driving the bacterium to  
16 spontaneously move into the nanopillars.<sup>68</sup> The interfacial energy gradient theory is applicable to  
17 materials with intrinsic contact angles between 30° and 60°,<sup>68</sup> which aligns with the contact angles  
18 of Si and PEGDMA used in this study (**Figure S1**). While this model does not explicitly account  
19 for polymer hydration or viscoelastic effects, it provides a useful framework for interpreting cell-  
20 nanopillar interactions.

21 Following the interfacial energy gradient theory, the driving force to induce bacterial  
22 adhesion and membrane expansion into the nanostructures and minimize the interfacial energy  
23 gradient<sup>13</sup> causes the suspended region of the bacterial membrane between initial contact points



1 with the top of nanostructures to experience a certain deformation, leading to a tensile force equal  
2 in magnitude and opposite in direction on the nanopillars. Thus, the stress imposed on the bacterial  
3 membrane can only be as large as the nanopillars can tolerate. Nanopillars that lack sufficient  
4 stiffness will be bent laterally towards the region of higher bacterial membrane stress, reducing the  
5 overall stress on the membrane, as they can no longer sustain the higher stress.

6 To confirm this hypothesis, the morphology of the bacteria and nanopillars was  
7 characterized using SEM. SEM imaging reveals morphological signatures of membrane  
8 deformation and rupture, which have been widely associated with mechanically induced  
9 bactericidal mechanisms in nanostructured surfaces. Qualitative analysis revealed that *E. coli*  
10 maintained an intact ellipsoidal shape on the flat surface (**Figure 4** and **Figure S2**), whereas many  
11 cells were damaged and flattened due to cytoplasm loss on the Si nanopillars, indicating the  
12 physical and mechanical bactericidal efficacy of Si nanopillars. Attributed to the high Young's  
13 modulus of Si (169 GPa),<sup>31</sup> the Si nanopillars had sufficient stiffness and did not deform  
14 underneath the damaged bacterial membrane. However, less drastic deformations of *E. coli* were  
15 observed on the PEGDMA nanopillars, indicating a lower possibility for cell damage and loss of  
16 cellular volume compared with cells on Si nanopillars. These observations corroborate the  
17 previous results from the bacterial live/dead assay. Moreover, the PEGDMA nanopillars adhered  
18 to the bacterial membrane showed bending towards the center of the bacteria, suggesting that the  
19 pressure applied to the bacterial membrane induces bending of nanopillars that lack sufficient  
20 stiffness along the direction of higher bacterial membrane stress.



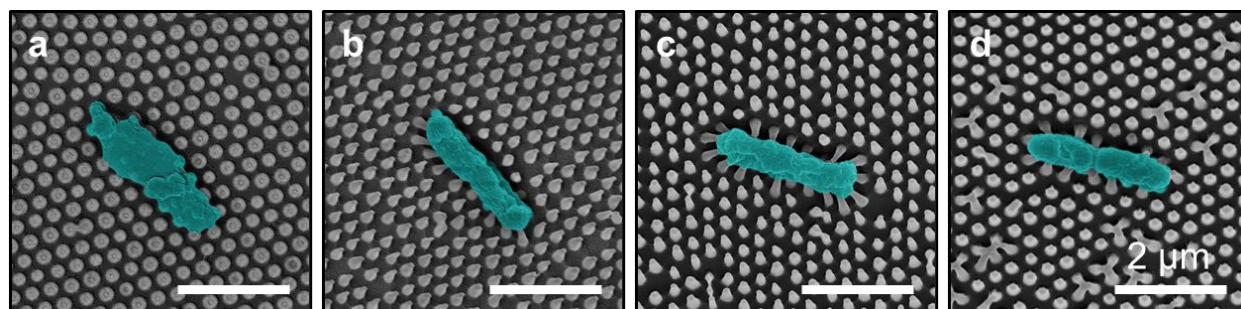


**Figure 4.** Top-view SEM images of *E. coli K12* incubated in a static incubator at 37 °C for 4 h on nanopillars of a) Si, PEGDMA with b) 4.5, c) 9, and d) 13.5 PEG repeating units. All scale bars are 2 μm.

To qualitatively evaluate the effect of nanopillar deformation on the bactericidal efficacy, Euler–Bernoulli beam theory was applied. In this theory, the resistance against bending, the bending modulus  $k_b$ , is proportional to the Young’s modulus of the material.<sup>69</sup>

$$k_b = \frac{3D^4}{64L^3} \pi E$$

The nanopillars were approximated as cylindrical beams using the tip diameter of 110 nm, recognizing that the tapered geometry may lead to a higher effective stiffness due to increased diameter toward the base. Nanopillars with a higher bending modulus showed higher resistance against deformation when similar forces were applied by the stress on the bacterial membrane (**Figure S3**), suggesting they can maintain their structure while contending with the stress on the bacterial membrane, while the nanopillars with lower bending moduli will be deformed upon application of this stress. Deformation of the nanopillars may reduce the localized stress exerted on the bacterial membrane while increasing contact area along the nanopillar sidewalls. This combination likely lowers the probability of membrane rupture and subsequent cell death.



1 Collectively, these observations suggest that decreased nanostructure stiffness diminished  
2 bactericidal efficacy against *E. coli* on nanopillar surfaces.

3  
4 **Understanding the Relationship between Nanopillar Stiffness and the Bactericidal Efficacy**  
5 **against *S. aureus*.**

6 To further understand the relationship between the nanopillar stiffness and bactericidal  
7 efficacy against Gram-positive strains, we evaluated the viability of *S. aureus*, one of the most  
8 common bacteria implicated in hospital infections,<sup>70</sup> on our surfaces by bacterial live/dead assays.  
9 **Figure 5a** shows the microscopic fluorescent images of stained *S. aureus* incubated on surfaces  
10 with nanopillars. We confirmed that 55 % of adhered *S. aureus* were stained with red fluorescence  
11 and damaged by Si nanopillars, while the percentage of non-viable cells on PEGDMA nanopillars  
12 decreased from 17 % to 14 % as their Young's moduli decreased from 190 MPa to 40 MPa (**Figure**  
13 **5b**). Surprisingly, the percentage of non-viable *S. aureus* increases to 41 % as the Young's modulus  
14 of nanopillars further decreases to 19 MPa. Fewer *S. aureus* bacteria were found on the PEGDMA  
15 nanopillars compared to those on Si, while no significant difference in the number of adhered  
16 bacteria was found amongst PEGDMA nanopillars with different stiffnesses (**Figure 5c**).



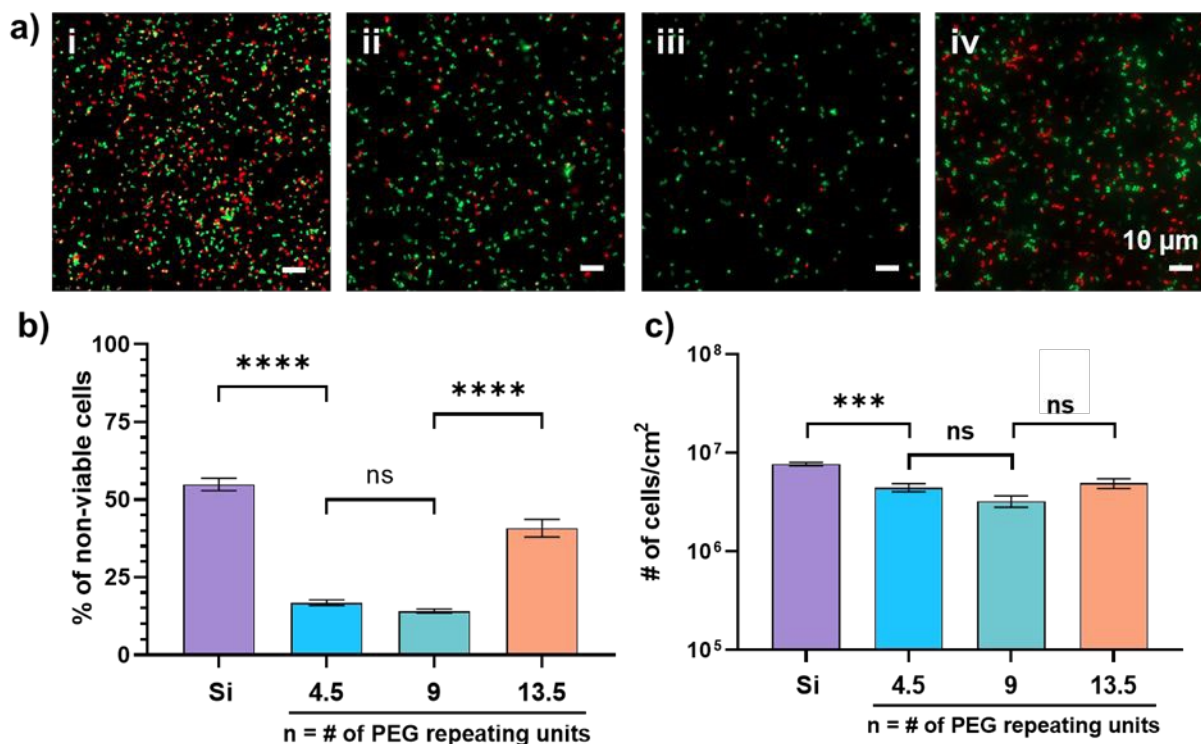
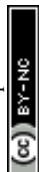
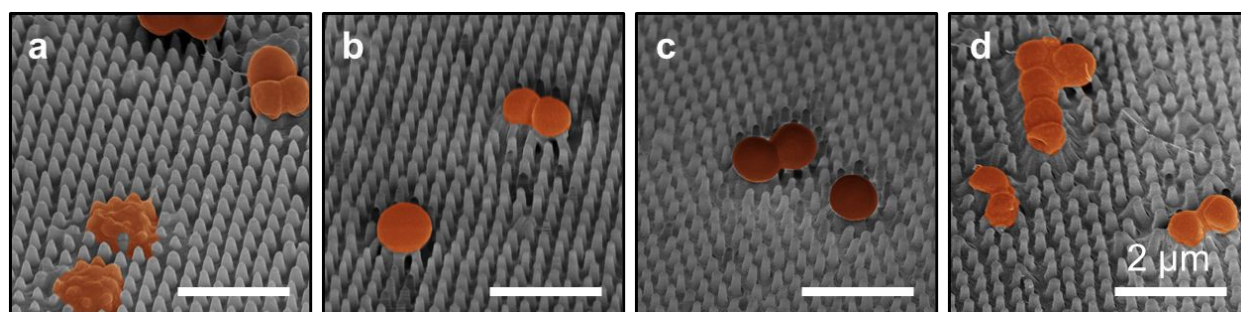


**Figure 5.** a) Representative fluorescent microscopic images of *S. aureus* on nanopillars of i) Si, ii) PEGDMA with 4.5, iii) 9, and iv) 13.5 PEG repeating units after 4 h cultivation in a static incubator at 37 °C. All scale bars are 10 μm. b) Quantitative image analysis on the percentage (%) of non-viable cells attached to the samples after 4 h of cultivation. c) Quantitative image analysis of the number of cells attached to the samples after 4 h of cultivation. (Data represent mean ± SEM, ns (not significant):  $p > 0.05$ ; \* $p < 0.05$ , \*\* $p < 0.01$ , \*\*\* $p < 0.001$ , \*\*\*\* $p < 0.0001$ )

Similarly, the force to drive *S. aureus* into the nanopillars and the accompanying pressure that can be applied to the bacterial membrane remained similar from the Si substrate to those made of PEGDMA, with the assumption that all nanopillars maintained their fabricated shape and structural integrity during the cell-nanopillar interaction.<sup>68</sup> However, the bactericidal efficacy observed on the nanopillars presented a different trend from this prediction, indicating that other



1 dominant factors exist to govern the bactericidal efficacy in the tested system. To further reveal  
2 potential factors affecting the bactericidal efficacy of the nanopillars, we characterized the  
3 morphology of *S. aureus* on the surfaces after 4 h of incubation by SEM (**Figure 6**). SEM images  
4 revealed that *S. aureus* cells on the Si nanopillars were embedded into the nanopillars with parts  
5 of their membranes lysed. This result corresponds to the bactericidal efficacy of Si nanopillars  
6 obtained from the bacterial live/dead assay, where approximately 55 % of the cells were found  
7 non-viable.



9  
10 **Figure 6.** Top-view SEM images of *S. aureus* incubated in a static incubator at 37 °C for 4 h on  
11 nanopillars of a) Si, PEGDMA with b) 4.5, c) 9, and d) 13.5 PEG repeating units. All scale bars  
12 are 2  $\mu\text{m}$ .

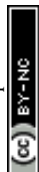
13  
14 We also observed that the bactericidal efficacy of Si nanopillars against *S. aureus* was  
15 lower than that against *E. coli* after 4 h of cultivation in solution. This is attributed to *S. aureus*  
16 having a stiffer membrane with a thicker layer of peptidoglycan compared to Gram-negative  
17 bacteria.<sup>71</sup> The thicker peptidoglycan layer offers a higher elastic modulus on the bacterial  
18 membrane, reducing the possibility of damage and rupture by nanopillars. Due to the stiffer  
19 membrane and bacterial congregation of *S. aureus*, the Si nanopillars with higher resistance to



1 bending were better able to maintain force on the bacterial membrane sufficient to damage or  
2 induce rupture.

3         Additionally, the SEM images, as well as the live/dead assay, show denser growth of *S.*  
4 *aureus* compared to *E. coli*. Staphylococci are known to form an aggressive biofilm that is difficult  
5 to eradicate, likely contributing to the increased growth and decreased bactericidal efficacy of *S.*  
6 *aureus* across all surfaces.<sup>72, 73</sup> Additionally, the adhesion mechanisms of *S. aureus* and *E. coli* to  
7 the PEGDMA nanopillars are governed by their unique cell structures and appendages.<sup>74</sup> In *S.*  
8 *aureus*, most adhesins are covalently linked to the cell wall peptidoglycan. Of these, the microbial  
9 surface components recognizing adhesive matrix molecules (MSCRAMMs) are primarily  
10 responsible for the strong binding of the bacterium to the surface.<sup>75</sup> Meanwhile, adhesion of *E. coli*  
11 to abiotic surfaces is aided by extracellular appendages such as type 1 fimbriae and curli amyloid  
12 fibers, contributing to their differences in adhesion dynamics.<sup>74</sup>

13         Initial bacterial adhesion is thought to be significantly influenced by physicochemical and  
14 electrostatic interactions between the surface and the bacterial envelope.<sup>76</sup> Surface hydrophobicity,  
15 often assessed via water contact angle, is commonly used as an indirect predictor of these  
16 interfacial interactions. While this metric does not fully capture the complexity of surface  
17 chemistry or hydration-layer effects, it provides a useful comparative framework for interpreting  
18 adhesion trends. In our system, the most hydrophilic sample (Si), as indicated by the lowest water  
19 contact angle (Figure S1), exhibited the highest adhesion density. For *E. coli*, adhesion density  
20 generally decreased as the nanostructured surface became more hydrophobic, with the exception  
21 of the 40 MPa sample. This trend is consistent with prior reports that the outer membrane of *E.*  
22 *coli* is predominantly hydrophilic, although it may vary depending on strain and local surface  
23 composition.<sup>77</sup> In contrast, *S. aureus*, which possesses a relatively hydrophobic cell wall,<sup>78</sup> showed



1 increased adhesion to more hydrophobic surfaces. This behavior aligns with the model proposed  
2 by Maikranz *et. al.* in which *S. aureus* adheres to hydrophobic surfaces through multiple weakly  
3 bonded macromolecules, compared to fewer but stronger interactions on hydrophilic surfaces.<sup>79</sup>  
4 Accordingly, the contributions of surface chemistry and protein adsorption to bacterial adhesion  
5 are recognized, but are not explicitly resolved within the scope of this study.

6 The motility of a bacterium also heavily influences adhesion dynamics, as bacteria must  
7 be close to the material's surface to overcome the energy barrier and bind to the surface.<sup>42</sup> In a  
8 previous study with *E. coli* K-12, engineered non-flagellated or paralyzed cells exhibited  
9 significantly weaker adhesion than the wild-type flagellated strain.<sup>80</sup> However, MRSA, generally  
10 considered non-motile, exhibited adhesion orders of magnitude higher than that of *E. coli*,  
11 indicating that motility is not a dominant factor in this system.

12 Our results indicate that the bactericidal efficacy of PEGDMA nanopillars against *S. aureus*  
13 decreased with increasing stiffness, whereas against *E. coli* it increased with nanopillar stiffness.  
14 Visualized in **Figures 6b and 6c**, many *S. aureus* cells were found to be intact and settled on top  
15 of the bent nanopillars of PEGDMA with Young's moduli of 190 MPa ( $n = 4.5$ ) and 40 MPa ( $n =$   
16 9). However, we found an exception when the Young's modulus of the nanopillars decreases  
17 further. We observed the highest number of non-viable *S. aureus* bacteria on nanopillars with the  
18 lowest stiffness ( $n = 13.5$ , 17 MPa) compared with substrates containing stiffer nanopillars.  
19 Moreover, many *S. aureus* cells were deformed and sank into the nanopillars, indicating a loss of  
20 cytoplasm and damage to the cellular integrity (**Figure 6d**). It is thought that the softest nanopillars  
21 cannot support *S. aureus* upon adhesion. This leads to the sinking of the spherical *S. aureus* (1-2  
22  $\mu\text{m}$  in diameter) into the nanopillars, a phenomenon not observed in the larger, rod-shaped *E. coli*  
23 (1-2  $\mu\text{m}$  length, 0.5  $\mu\text{m}$  width). Due to the 350 nm distance between nanopillars and the higher



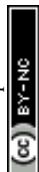
1 elastic modulus of the peptidoglycan layer, *S. aureus* is able to exert enough force to bend the  
2 softer nanopillars and create enough space to situate in-between nanopillars. Along with sinking,  
3 the interactive radius on the substrate increases due to the spherical shape of *S. aureus*, leading to  
4 greater adhesion to the sidewalls of nanopillars around the bacterium's perimeter.

5         Based on the Euler–Bernoulli beam theory, we know that the bending modulus,  $k_b$ , is  
6 inversely proportional to the third power of the height of the point of action. Thus, adhesion to  
7 multiple sidewalls of the nanopillars significantly increases lateral interaction between the  
8 bacterial membrane and the nanopillars, providing greater resistance to bending and enhancing  
9 bactericidal efficacy (**Figure 5b and Figure 6d**). Choi *et al.* also reported comparable behavior,  
10 showing that *S. aureus* can be captured and killed by lateral stretching when attached to nanopillar  
11 sidewalls spaced similarly to the cell size.<sup>81</sup> The lateral compression of *S. aureus* by the nanopillars  
12 results in increased bactericidal efficacy in softer, more deformable nanopillars with lower  
13 Young's moduli, where the bacterium is able to sink lower into the nanopillars and increase this  
14 interaction. The reverse holds for the effect on *E. coli*: the rod-shaped bacterium, with a less-rigid  
15 outer membrane, adheres on top of the nanopillars. Here, stiffer nanopillars can exert sufficient  
16 force on *E. coli* to puncture the outer membrane without bending. To our best knowledge, our  
17 results first confirmed that bactericidal efficacy is affected not only by nanopillar stiffness but also  
18 by changes in interactions arising from reductions in nanopillar stiffness and cellular size.

19

## 20 **Understanding the Relationship between Nanopillar Stiffness and the Surface-tension-** 21 **driven Bactericidal Efficacy against Gram-negative and Gram-positive Bacteria.**

22         As the *E. coli* and *S. aureus* are incubated in solution, the interfacial energy gradient plays  
23 an important role in driving the bacteria into the nanopillars, leading to bacterial membrane

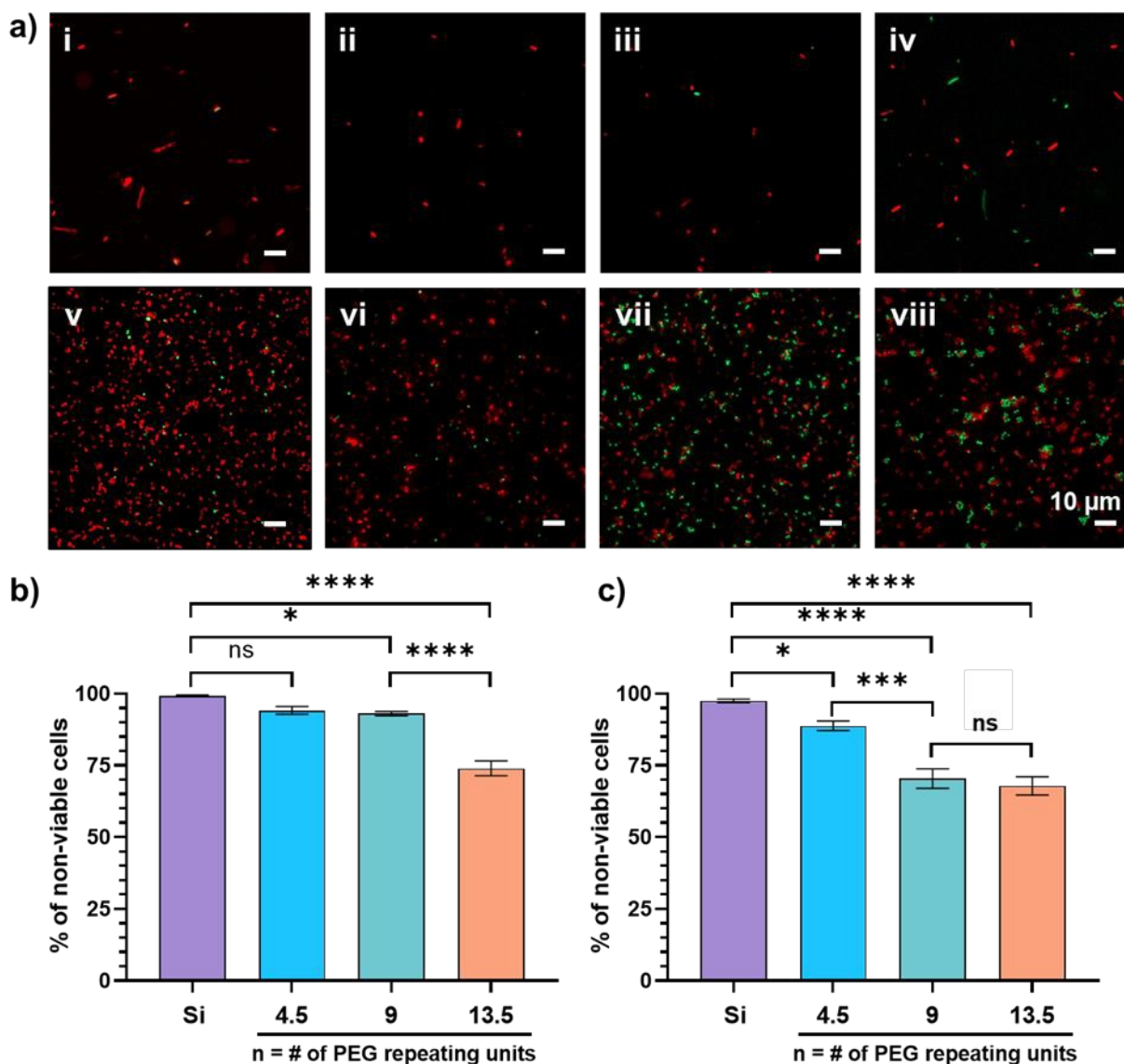


1 damage and subsequent death. However, as observed in the evaluation of bactericidal efficacy in  
2 solution, only up to 65 % of *E. coli* and 55 % of *S. aureus* cells adhering to the nanopillars were  
3 inactivated. To further enhance the bactericidal efficacy on the nanopillars, an external force  
4 towards the substrate was introduced to the system by the surface tension of the air-liquid interface  
5 along the bacterial membrane during surface water evaporation. This creates an additional driving  
6 force to pull the bacteria towards the nanopillars, leading to cell rupture on the nanopillars by  
7 imposing pressure on the bacterial membrane until it yields to its elastic modulus.<sup>55</sup>

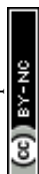
8         Considering that nanopillar stiffness can also affect bactericidal efficacy under external  
9 force, we further evaluated the enhancement of bactericidal efficacy against *E. coli* and *S. aureus*  
10 on nanopillars with different stiffness upon introduction of an external force. **Figure 7a** shows the  
11 representative fluorescent images of *E. coli* and *S. aureus* upon an external force induced by  
12 surface tension during a short exposure of surfaces to air. Based on quantitative image analysis,  
13 we found that bactericidal efficacy against *E. coli* and *S. aureus* was significantly enhanced on Si  
14 nanopillars, reaching 99 % and 97 %, respectively (**Figure 7b and 7c**). This enhancement can be  
15 understood by imposing an additional driving force arising from surface tension to increase the  
16 stress on the bacterial membrane, thereby increasing the likelihood of cell rupture and damage.<sup>55</sup>

17





1  
2 **Figure 7.** a) Representative fluorescent microscopic images of *E. coli* on nanopillars of i) Si,  
3 PEGDMA with ii) 4.5, iii) 9, and iv) 13.5 PEG repeating units after 4 h cultivation in a static  
4 incubator at 37  $^{\circ}\text{C}$  followed by 60 s drying in air. v)-viii) respective fluorescent images of *S. aureus*  
5 on the samples with same treatment. Scale bars are 10  $\mu\text{m}$ . Quantitative image analysis on percent  
6 (%) of non-viable b) *E. coli* and c) *S. aureus* attached on the samples after 4 h of culture and 60 s  
7 drying in air. (Data represent mean  $\pm$  SEM, ns (not significant):  $p > 0.05$ ; \* $p < 0.05$ , \*\* $p < 0.01$ ,  
8 \*\*\* $p < 0.001$ , \*\*\*\* $p < 0.0001$ )

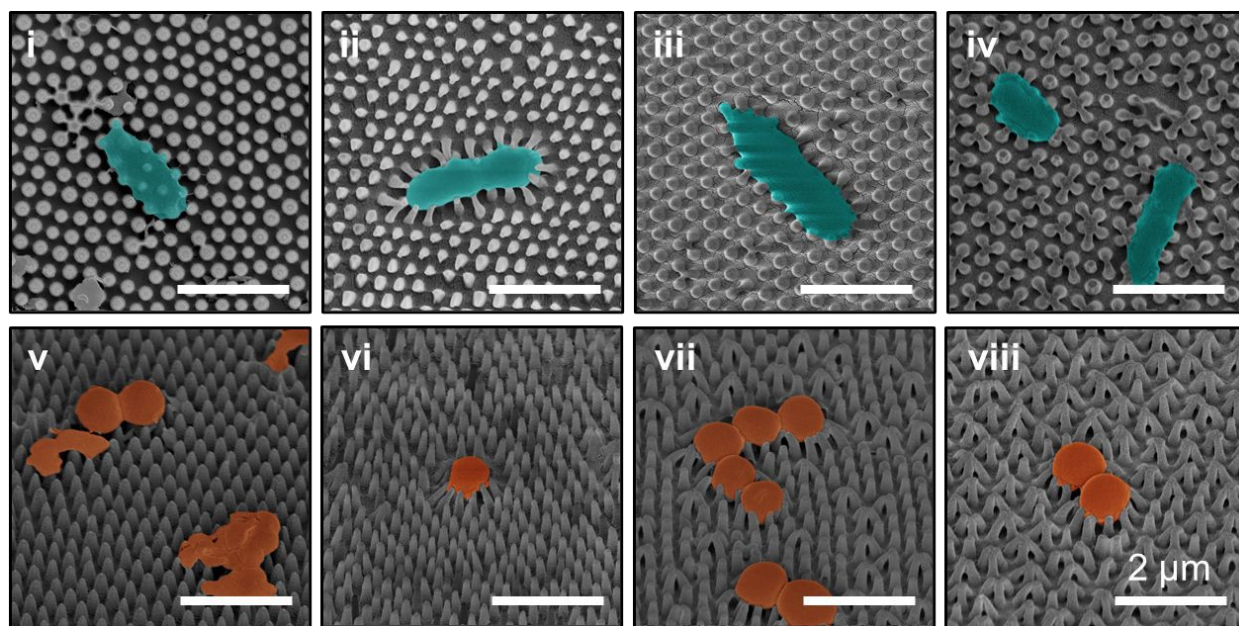


1 To better understand the effect of the surface-tension-induced external force on the  
2 bactericidal efficacy against different strains, we calculated the external force and pressure applied  
3 to the bacterial membrane as a function of the relative liquid level during water evaporation (**Table**  
4 **S2** and **Figure S4**). In the calculation, the force is calculated by integrating surface tension along  
5 the periphery of the cells, and the pressure is calculated by dividing the force by the projected area  
6 in contact with a cylindrical post. The force and pressure reach a maximum when the liquid level  
7 is near the half-height of the cells due to surface tension interacting with more bacterial membranes  
8 along the cell's perimeter than at other heights. We also noticed that a lower external force was  
9 generated with the smaller *S. aureus* compared to the larger *E. coli*. However, due to the higher  
10 ratio between perimeter and area of *S. aureus* compared to *E. coli*, a higher force is applied on the  
11 unit area of *S. aureus*, causing higher pressure applied on the membrane of *S. aureus*. Thus, similar  
12 bactericidal efficacy against *S. aureus* and *E. coli* was observed on Si nanopillars, despite the fact  
13 that *S. aureus* has a stiffer bacterial membrane. Moreover, we found that trials with *S. aureus*  
14 exhibited lower bactericidal efficacy on the corresponding soft nanopillars than those with *E. coli*.  
15 Analogous to bactericidal efficacy in solution, surface-tension-driven bactericidal efficacies are  
16 reduced as the nanopillar stiffness decreases. We hypothesized that nanopillars with lower stiffness  
17 were further deformed upon the introduction of the external force, leading to an inclination of the  
18 nanopillars and a change in the cell-nanopillar interaction. As a result, the percentage of non-viable  
19 *E. coli* and *S. aureus* cells was reduced on the soft nanopillars.

20 To confirm this hypothesis, we characterized the morphology of *E. coli* and *S. aureus* on  
21 nanopillars by SEM. *E. coli* and *S. aureus* are intact on a flat surface (**Figure S5**) but were lysed  
22 on Si nanopillars (**Figure 8**). These results of drastic cell morphology changes on the Si nanopillars  
23 confirm that imposing external force enhances the deformation of adhered bacteria and the



1 bactericidal efficacy. Similarly, bacteria sank into PEGDMA nanopillars upon the addition of the  
2 external force, and the surrounding nanopillars inclined directionally towards the bacteria. The  
3 stiffer nanopillars, possessing higher resistance to bending, result in larger tension on the bacterial  
4 membrane and thus greater bactericidal efficacy. Moreover, the agglomeration of nanopillars was  
5 observed on the PEGDMA surface with the lowest stiffness, which is attributed to adhesion-  
6 mediated elastocapillary interactions during water evaporation on the surface.<sup>82</sup> Due to the  
7 agglomeration, the bacterial membrane has a possibility to settle on the side of the nanopillars,  
8 which leads to an increase in the contact area and a decrease in the pressure applied to the bacterial  
9 membrane. Eventually, the bactericidal efficacy against *E. coli* and *S. aureus* decreases on the  
10 nanopillars with low stiffness. These observations further confirm the previously mentioned  
11 hypothesis.



12  
13 **Figure 8.** Top-view SEM images of *E. coli* on nanopillars of i) Si, PEGDMA with ii) 4.5, iii) 9,  
14 and iv) 13.5 PEG repeating units after 4 h cultivation in a static incubator at 37 °C followed by 60  
15 s drying in air. v)-viii) respective tilted-view SEM images of *S. aureus* on the samples with same  
16 treatment. All scale bars are 2 μm.



1 While this study provides insight into the role of nanopillar stiffness in bactericidal efficacy,  
2 several considerations should be noted to contextualize the scope of the work. Tuning the Young's  
3 modulus of PEGDMA thin films through crosslinking density may also influence polymer  
4 hydration and viscoelastic properties, which could contribute to bacteria–surface interactions  
5 alongside stiffness effects. In addition, the proposed bactericidal mechanisms are inferred from  
6 qualitative morphological observations and analytical modeling; direct measurements of  
7 interaction forces would provide further mechanistic resolution. The present study focuses on  
8 short-term behavior to probe primary bacterial adhesion, using two representative bacterial strains  
9 and a single nanostructure geometry to enable controlled comparison of stiffness-dependent trends.  
10 The selected nanopillar geometry and density were based on our previous work, in which these  
11 parameters were optimized to achieve high bactericidal efficacy against *E. coli*. While surface-  
12 tension-driven bactericidal effects demonstrate enhanced efficacy under drying conditions, their  
13 influence may vary in fully hydrated environments. Within this context, the results establish a  
14 foundation for understanding stiffness-dependent bactericidal behavior and provide guiding  
15 principles for the design of mechanically tunable antibacterial surfaces.



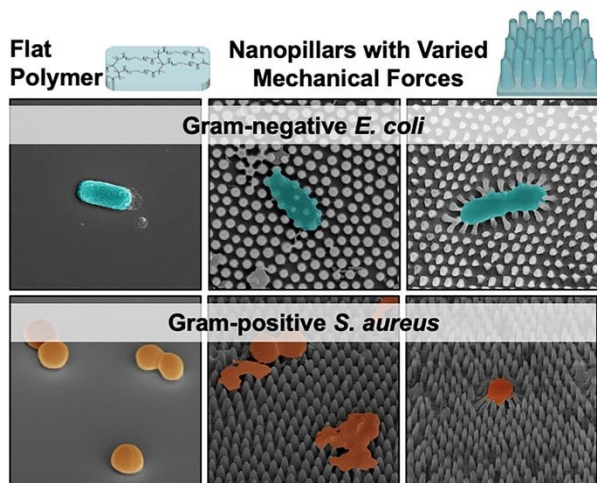
## 1 CONCLUSION

2           In this work, we investigated the effect of nanopillars' stiffness on the bactericidal efficacy  
3 against Gram-negative and Gram-positive bacteria. Nanostructured PEGDMA thin films with  
4 tunable Young's moduli were fabricated by varying crosslinking density, enabling evaluation of  
5 stiffness-dependent trends while maintaining similar geometric features. Using *E. coli* K12 and  
6 methicillin-resistant *Staphylococcus aureus* (MRSA) as representative models, we observed that  
7 bactericidal efficacy against *E. coli* decreased with decreasing nanopillar stiffness, consistent with  
8 reduced mechanical interaction between softer nanopillars and the bacterial membrane. In contrast,  
9 nanopillars with both high and low stiffness exhibited strong bactericidal activity against *S. aureus*,  
10 suggesting that bactericidal performance depends not only on nanostructure stiffness but also on  
11 bacterial properties such as size and cell envelope structure. Moreover, the introduction of an  
12 external force via surface tension was found to enhance bactericidal efficacy, with greater  
13 enhancement observed for stiffer nanopillars. These findings suggest that nanopillar stiffness  
14 influences bactericidal performance under both passive and externally driven conditions. It should  
15 be noted, however, that direct quantification of force and membrane stress will further refine the  
16 mechanistic understanding of these interactions. This work provides insight into cell-structure  
17 interactions and rational designs for creating synergistic antibacterial nanostructures on materials  
18 with different mechanical properties. Longer-term efforts will aim to translate these findings into  
19 novel antibacterial surfaces to combat industrial biofouling and medical device infection.

20



## 1 Table of Content Image



2



1 ASSOCIATED CONTENT

2 **Supporting Information.**

3 AUTHOR INFORMATION

4 **Corresponding Author**

5 \*Yeongseon Jang: [y.jang@ufl.edu](mailto:y.jang@ufl.edu)

6 **Author Contributions**

7 The manuscript was written through the contributions of all authors. R. Tan and E. Thomas  
8 contributed equally and share first authorship. All authors have given approval to the final version  
9 of the manuscript.

10 **Funding Sources**

11 This research was financially supported by Prof. Jang's startup funds (19030100-211-CRRNT-  
12 00128948) provided by the Department of Chemical Engineering and Herbert Wertheim College  
13 of Engineering at the University of Florida.

14 **Notes**

15 The authors declare no competing financial interest.

16 **ACKNOWLEDGMENT**

17 The authors acknowledge Prof. Thomas Angelini (UF, Mechanical and Aerospace Engineering)  
18 for his assistance in using the micro-indenter for measuring mechanical properties and Prof.  
19 Kwangcheol Jeong (UF, Microbiology) for providing the cell strains used in this study.



## 1 REFERENCES

- 2 1. Linklater, D. P.; Baulin, V. A.; Juodkazis, S.; Crawford, R. J.; Stoodley, P.; Ivanova,  
3 E. P., Mechano-bactericidal actions of nanostructured surfaces. *Nature Reviews Microbiology*  
4 **2021**, *19* (1), 8-22.
- 5 2. Sauer, K.; Stoodley, P.; Goeres, D. M.; Hall-Stoodley, L.; Burmølle, M.; Stewart, P.  
6 S.; Bjarnsholt, T., The biofilm life cycle: expanding the conceptual model of biofilm formation.  
7 *Nature Reviews Microbiology* **2022**, *20* (10), 608-620.
- 8 3. Liu, Y.; Zhao, Q., Influence of surface energy of modified surfaces on bacterial adhesion.  
9 *Biophysical Chemistry* **2005**, *117* (1), 39-45.
- 10 4. Lu, Z.; Mondarte, E. A. Q.; Suthiwanich, K.; Hayashi, T.; Masuda, T.; Isu, N.; Takai,  
11 M., Study on Bacterial Antiadhesiveness of Stiffness and Thickness Tunable Cross-Linked  
12 Phospholipid Copolymer Thin-Film. *ACS Applied Bio Materials* **2020**, *3* (2), 1079-1087.
- 13 5. Yang, X.; Hou, J.; Tian, Y.; Zhao, J.; Sun, Q.; Zhou, S., Antibacterial surfaces:  
14 Strategies and applications. *Science China Technological Sciences* **2022**, *65* (5), 1000-1010.
- 15 6. Chouirfa, H.; Bouloussa, H.; Migonney, V.; Falentin-Daudré, C., Review of titanium  
16 surface modification techniques and coatings for antibacterial applications. *Acta Biomaterialia*  
17 **2019**, *83*, 37-54.
- 18 7. Ventola, C. L., The antibiotic resistance crisis: part 1: causes and threats. *Pharmacy and*  
19 *therapeutics* **2015**, *40* (4), 277.
- 20 8. Mah, T.-F. C.; O'Toole, G. A., Mechanisms of biofilm resistance to antimicrobial agents.  
21 *Trends in microbiology* **2001**, *9* (1), 34-39.
- 22 9. Prabhu, S.; Poulouse, E. K., Silver nanoparticles: mechanism of antimicrobial action,  
23 synthesis, medical applications, and toxicity effects. *International nano letters* **2012**, *2* (1), 1-10.
- 24 10. Tan, R.; Yoo, J.; Jang, Y., Engineering Approaches to Create Antibacterial Surfaces on  
25 Biomedical Implants and Devices. *Racing for the Surface* **2020**, 313-340.
- 26 11. Hasan, J.; Crawford, R. J.; Ivanova, E. P., Antibacterial surfaces: the quest for a new  
27 generation of biomaterials. *Trends in biotechnology* **2013**, *31* (5), 295-304.
- 28 12. Ivanova, E. P.; Hasan, J.; Webb, H. K.; Truong, V. K.; Watson, G. S.; Watson, J. A.;  
29 Baulin, V. A.; Pogodin, S.; Wang, J. Y.; Tobin, M. J., Natural bactericidal surfaces: mechanical  
30 rupture of *Pseudomonas aeruginosa* cells by cicada wings. *Small* **2012**, *8* (16), 2489-2494.
- 31 13. Pogodin, S.; Hasan, J.; Baulin, V. A.; Webb, H. K.; Truong, V. K.; Nguyen, T. H. P.;  
32 Boshkovikj, V.; Fluke, C. J.; Watson, G. S.; Watson, J. A., Biophysical model of bacterial cell  
33 interactions with nanopatterned cicada wing surfaces. *Biophysical journal* **2013**, *104* (4), 835-  
34 840.
- 35 14. Ivanova, E. P.; Hasan, J.; Webb, H. K.; Gervinskas, G.; Juodkazis, S.; Truong, V. K.;  
36 Wu, A. H.; Lamb, R. N.; Baulin, V. A.; Watson, G. S., Bactericidal activity of black silicon.  
37 *Nature communications* **2013**, *4* (1), 1-7.
- 38 15. Truong, V.; Geeganagamage, N.; Baulin, V.; Vongsvivut, J.; Tobin, M.; Luque, P.;  
39 Crawford, R.; Ivanova, E., The susceptibility of *Staphylococcus aureus* CIP 65.8 and  
40 *Pseudomonas aeruginosa* ATCC 9721 cells to the bactericidal action of nanostructured  
41 *Calopteryx haemorrhoidalis* damselfly wing surfaces. *Applied Microbiology & Biotechnology*  
42 **2017**, *101* (11), 4683-4690.
- 43 16. Li, X.; Cheung, G.; Watson, G.; Watson, J.; Lin, S.; Schwarzkopf, L.; Green, D., The  
44 nanotipped hairs of gecko skin and biotemplated replicas impair and/or kill pathogenic bacteria  
45 with high efficiency. *Nanoscale* **2016**, *8* (45), 18860-18869.



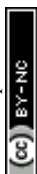
- 1 17. Han, S.; Ji, S.; Abdullah, A.; Kim, D.; Lim, H.; Lee, D., Superhydrophilic nanopillar-  
2 structured quartz surfaces for the prevention of biofilm formation in optical devices. *Applied*  
3 *Surface Science* **2018**, *429*, 244-252.
- 4 18. Linklater, D. P.; Juodkazis, S.; Crawford, R. J.; Ivanova, E. P., Mechanical inactivation  
5 of *Staphylococcus aureus* and *Pseudomonas aeruginosa* by titanium substrata with hierarchical  
6 surface structures. *Materialia* **2019**, *5*, 100197.
- 7 19. Bhadra, C. M.; Truong, V. K.; Pham, V. T.; Al Kobaisi, M.; Seniutinas, G.; Wang, J.  
8 Y.; Juodkazis, S.; Crawford, R. J.; Ivanova, E. P., Antibacterial titanium nano-patterned arrays  
9 inspired by dragonfly wings. *Scientific reports* **2015**, *5* (1), 1-12.
- 10 20. Jang, Y.; Choi, W. T.; Johnson, C. T.; García, A. J.; Singh, P. M.; Breedveld, V.;  
11 Hess, D. W.; Champion, J. A., Inhibition of bacterial adhesion on nanotextured stainless steel  
12 316L by electrochemical etching. *ACS biomaterials science & engineering* **2018**, *4* (1), 90-97.
- 13 21. Reed, J. H.; Gonsalves, A. E.; Román, J. K.; Oh, J.; Cha, H.; Dana, C. E.; Toc, M.;  
14 Hong, S.; Hoffman, J. B.; Andrade, J. E., Ultrascaleable multifunctional nanoengineered copper  
15 and aluminum for antiadhesion and bactericidal applications. *ACS Applied Bio Materials* **2019**, *2*  
16 (7), 2726-2737.
- 17 22. Elbourne, A.; Coyle, V. E.; Truong, V. K.; Sabri, Y. M.; Kandjani, A. E.; Bhargava, S.  
18 K.; Ivanova, E. P.; Crawford, R. J., Multi-directional electrodeposited gold nanospikes for  
19 antibacterial surface applications. *Nanoscale Advances* **2019**, *1* (1), 203-212.
- 20 23. Dickson, M. N.; Liang, E. I.; Rodriguez, L. A.; Vollereaux, N.; Yee, A. F.,  
21 Nanopatterned polymer surfaces with bactericidal properties. *Biointerphases* **2015**, *10* (2),  
22 021010.
- 23 24. Elbourne, A.; Chapman, J.; Gelmi, A.; Cozzolino, D.; Crawford, R. J.; Truong, V. K.,  
24 Bacterial-nanostructure interactions: The role of cell elasticity and adhesion forces. *Journal of*  
25 *colloid and interface science* **2019**, *546*, 192-210.
- 26 25. Modaresifar, K.; Azizian, S.; Ganjian, M.; Fratila-Apachitei, L. E.; Zadpoor, A. A.,  
27 Bactericidal effects of nanopatterns: a systematic review. *Acta biomaterialia* **2019**, *83*, 29-36.
- 28 26. Tan, R.; Marzolini, N.; Jiang, P.; Jang, Y., Bio-Inspired Polymer Thin Films with Non-  
29 Close-Packed Nanopillars for Enhanced Bactericidal and Antireflective Properties. *ACS Applied*  
30 *Polymer Materials* **2020**, *2* (12), 5808-5816.
- 31 27. Cui, Q.; Liu, T.; Li, X.; Song, K.; Ge, D., Nanopillared Polycarbonate Surfaces Having  
32 Variable Feature Parameters as Bactericidal Coatings. *ACS Applied Nano Materials* **2020**, *3* (5),  
33 4599-4609.
- 34 28. Davey, M. E.; O'toole, G. A., Microbial Biofilms: from Ecology to Molecular Genetics.  
35 *Microbiology and Molecular Biology Reviews* **2000**, *64* (4), 847-867.
- 36 29. Shamis, Y.; Taube, A.; Shramkov, Y.; Mitik-Dineva, N.; Vu, B.; Ivanova, E. P.,  
37 Development of a microwave treatment technique for bacterial decontamination of raw meat.  
38 *International Journal of Food Engineering* **2008**, *4* (3), Article 8.
- 39 30. Michalska, M.; Gambacorta, F.; Divan, R.; Aranson, I. S.; Sokolov, A.; Noirot, P.;  
40 Laible, P. D., Tuning antimicrobial properties of biomimetic nanopatterned surfaces. *Nanoscale*  
41 **2018**, *10* (14), 6639-6650.
- 42 31. Hopcroft, M. A.; Nix, W. D.; Kenny, T. W., What is the Young's Modulus of Silicon?  
43 *Journal of microelectromechanical systems* **2010**, *19* (2), 229-238.
- 44 32. Wong, E. W.; Sheehan, P. E.; Lieber, C. M., Nanobeam mechanics: elasticity, strength,  
45 and toughness of nanorods and nanotubes. *science* **1997**, *277* (5334), 1971-1975.



- 1 33. Ivanova, E. P.; Linklater, D. P.; Werner, M.; Baulin, V. A.; Xu, X.; Vrancken, N.;  
2 Rubanov, S.; Hanssen, E.; Wandiyanto, J.; Truong, V. K., The multi-faceted mechano-  
3 bactericidal mechanism of nanostructured surfaces. *Proceedings of the National Academy of*  
4 *Sciences* **2020**, *117* (23), 12598-12605.
- 5 34. Linklater, D. P.; De Volder, M.; Baulin, V. A.; Werner, M.; Jessl, S.; Golozar, M.;  
6 Maggini, L.; Rubanov, S.; Hanssen, E.; Juodkasis, S., High aspect ratio nanostructures kill  
7 bacteria via storage and release of mechanical energy. *ACS nano* **2018**, *12* (7), 6657-6667.
- 8 35. Lohmann, S. C.; Tripathy, A.; Milionis, A.; Keller, A.; Poulikakos, D., Effect of  
9 Flexibility and Size of Nanofabricated Topographies on the Mechanobactericidal Efficacy of  
10 Polymeric Surfaces. *ACS Applied Bio Materials* **2022**, *5* (4), 1564-1575.
- 11 36. Park, H.-H.; Sun, K.; Seong, M.; Kang, M.; Park, S.; Hong, S.; Jung, H.; Jang, J.;  
12 Kim, J.; Jeong, H. E., Lipid-hydrogel-nanostructure hybrids as robust biofilm-resistant polymeric  
13 materials. *ACS Macro Letters* **2018**, *8* (1), 64-69.
- 14 37. Park, S.; Park, H.-H.; Sun, K.; Gwon, Y.; Seong, M.; Kim, S.; Park, T.-E.; Hyun, H.;  
15 Choung, Y.-H.; Kim, J., Hydrogel nanospine patch as a flexible anti-pathogenic scaffold for  
16 regulating stem cell behavior. *ACS nano* **2019**, *13* (10), 11181-11193.
- 17 38. Kim, H.-K.; Cho, Y.-S.; Park, H.-H., PEGDMA-Based Pillar-Shape Nanostructured  
18 Antibacterial Films Having Mechanical Robustness. *ACS Applied Bio Materials* **2022**, *5* (6),  
19 3006-3012.
- 20 39. Peng, L.; Chang, L.; Liu, X.; Lin, J.; Liu, H.; Han, B.; Wang, S., Antibacterial  
21 Property of a Polyethylene Glycol-Grafted Dental Material. *ACS Applied Materials & Interfaces*  
22 **2017**, *9* (21), 17688-17692.
- 23 40. Kang, N.-U.; Kim, G. H.; Kim, H.-K.; Kim, S. H.; Kim, Y. Y.; Park, H.-H.; Cho, Y.-  
24 S., Poly(ethylene glycol) dimethacrylate (PEGDMA) multi-functional pillar-patterned surface for  
25 osteogenic differentiation of pre-osteoblast and anti-bacterial effects to Escherichia coli and  
26 Staphylococcus aureus. *Surfaces and Interfaces* **2024**, *55*, 105221.
- 27 41. Kolewe, K. W.; Peyton, S. R.; Schiffman, J. D., Fewer Bacteria Adhere to Softer  
28 Hydrogels. *ACS Applied Materials & Interfaces* **August 26, 2015**, *7* (35), 19562-19569.
- 29 42. Hori, K.; Matsumoto, S., Bacterial adhesion: From mechanism to control. *Biochemical*  
30 *Engineering Journal* **2010**, *48* (3), 424-434.
- 31 43. Min, W. L.; Jiang, B.; Jiang, P., Bioinspired self - cleaning antireflection coatings.  
32 *Advanced Materials* **2008**, *20* (20), 3914-3918.
- 33 44. Levenson, M.D., Viswanathan, N.S., Simpson, R.A., Improving resolution in  
34 photolithography with a phase-shifting mask. *IEEE Transactions on Electron Devices* **1982**, *29*  
35 (12), 1828-1836.
- 36 45. Vieu, C.; Carcenac, F.; Pépin, A.; Chen, Y.; Mejias, M.; Lebib, A.; Manin-Ferlazzo,  
37 L.; Couraud, L.; Launois, H., Electron beam lithography: resolution limits and applications.  
38 *Applied Surface Science* **2000**, *164* (1-4).
- 39 46. Melngailis, J., Focused ion beam technology and applications. *Journal of Vacuum*  
40 *Science & Technology B: Microelectronics Processing and Phenomena* **1987**, *5* (2), 469-495.
- 41 47. Younan Xia; John A. Rogers; Kateri E. Paul, a.; George M. Whitesides\*,  
42 Unconventional Methods for Fabricating and Patterning Nanostructures **1999**, *99* (7), 1823-1848.
- 43 48. Chou, S. Y.; Krauss, P. R.; Renstrom, P. J., Imprint Lithography with 25-Nanometer  
44 Resolution. *Science* **1996**, *272* (5258), 85-87.
- 45 49. Wang, Y.; Zhang, M.; Lai, Y.; Chi, L., Advanced colloidal lithography: From patterning  
46 to applications. *Nano Today* **2018**, *22*, 36-61.



- 1 50. Stöber, W.; Fink, A.; Bohn, E., Controlled growth of monodisperse silica spheres in the  
2 micron size range. *Journal of colloid and interface science* **1968**, *26* (1), 62-69.
- 3 51. Garcia, M.; Schulze, K. D.; O'Bryan, C. S.; Bhattacharjee, T.; Sawyer, W. G.;  
4 Angelini, T. E., Eliminating the surface location from soft matter contact mechanics  
5 measurements. *Tribology-Materials, surfaces & interfaces* **2017**, *11* (4), 187-192.
- 6 52. Kothary, P.; Phillips, B. M.; Leo, S.-Y.; Jiang, P., Bioinspired broadband  
7 midwavelength infrared antireflection coatings on silicon. *Journal of Vacuum Science &*  
8 *Technology B, Nanotechnology and Microelectronics: Materials, Processing, Measurement, and*  
9 *Phenomena* **2016**, *34* (4), 041807.
- 10 53. Antonov, P. V.; Zuiddam, M. R.; Frenken, J. W., Fabrication of high-aspect ratio silicon  
11 nanopillars for tribological experiments. *Journal of Micro/Nanolithography, MEMS, and*  
12 *MOEMS* **2015**, *14* (4), 044506.
- 13 54. Heo, S. Y.; Koh, J. K.; Kang, G.; Ahn, S. H.; Chi, W. S.; Kim, K.; Kim, J. H.,  
14 Bifunctional moth - eye nanopatterned dye - sensitized solar cells: light - harvesting and self -  
15 cleaning effects. *Advanced Energy Materials* **2014**, *4* (3), 1300632.
- 16 55. Valiei, A.; Lin, N.; Bryche, J.-F.; McKay, G.; Canva, M.; Charette, P. G.; Nguyen,  
17 D.; Moraes, C.; Tufenkji, N., Hydrophilic mechano-bactericidal nanopillars require external  
18 forces to rapidly kill bacteria. *Nano letters* **2020**, *20* (8), 5720-5727.
- 19 56. Killion, J. A.; Geever, L. M.; Devine, D. M.; Kennedy, J. E.; Higginbotham, C. L.,  
20 Mechanical properties and thermal behaviour of PEGDMA hydrogels for potential bone  
21 regeneration application. *Journal of the mechanical behavior of biomedical materials* **2011**, *4*  
22 (7), 1219-1227.
- 23 57. Patel, N. R.; Whitehead, A. K.; Newman, J. J.; Caldorera-Moore, M. E., Poly (ethylene  
24 glycol) hydrogels with tailorable surface and mechanical properties for tissue engineering  
25 applications. *Acs Biomaterials Science & Engineering* **2017**, *3* (8), 1494-1498.
- 26 58. Killion, J. A.; Geever, L. M.; Devine, D. M.; Grehan, L.; Kennedy, J. E.;  
27 Higginbotham, C. L., Modulating the mechanical properties of photopolymerised polyethylene  
28 glycol-polypropylene glycol hydrogels for bone regeneration. *Journal of Materials Science*  
29 **2012**, *47* (18), 6577-6585.
- 30 59. Burke, G.; Barron, V.; Geever, T.; Geever, L.; Devine, D. M.; Higginbotham, C. L.,  
31 Evaluation of the materials properties, stability and cell response of a range of PEGDMA  
32 hydrogels for tissue engineering applications. *Journal of the Mechanical Behavior of Biomedical*  
33 *Materials* **2019**, *99*, 1-10.
- 34 60. Ortega, A. M.; Kasprzak, S. E.; Yakacki, C. M.; Diani, J.; Greenberg, A. R.; Gall, K.,  
35 Structure - property relationships in photopolymerizable polymer networks: Effect of  
36 composition on the crosslinked structure and resulting thermomechanical properties of a (meth)  
37 acrylate - based system. *Journal of applied polymer science* **2008**, *110* (3), 1559-1572.
- 38 61. Kolewe, K. W.; Zhu, J.; Mako, N. R.; Nonnenmann, S. S.; Schiffman, J. D., Bacterial  
39 Adhesion Is Affected by the Thickness and Stiffness of Poly(ethylene glycol) Hydrogels. *ACS*  
40 *Applied Materials & Interfaces* **2018**, *10* (3), 2275-2281.
- 41 62. Techakasikornpanich, M.; Jangpatarapongsa, K.; Polpanich, D.; Elaissari, A., Impact of  
42 polymeric films and hydrogels: Physical characteristics on bacterial growth. *Polymers for*  
43 *Advanced Technologies* **2024**, *35* (2), e6311.
- 44 63. Teng, L.; Lee, S.; Ginn, A.; Markland, S. M.; Mir, R. A.; DiLorenzo, N.; Boucher, C.;  
45 Prospero, M.; Johnson, J.; Morris Jr, J. G., Genomic comparison reveals natural occurrence of



- 1 clinically relevant multidrug-resistant extended-spectrum- $\beta$ -lactamase-producing *Escherichia*  
2 *coli* strains. *Applied and environmental microbiology* **2019**, *85* (13), e03030-18.
- 3 64. Song, F.; Koo, H.; Ren, D., Effects of material properties on bacterial adhesion and  
4 biofilm formation. *Journal of dental research* **2015**, *94* (8), 1027-1034.
- 5 65. Boulos, L.; Prevost, M.; Barbeau, B.; Coallier, J.; Desjardins, R., LIVE/DEAD®  
6 BacLight™: application of a new rapid staining method for direct enumeration of viable and  
7 total bacteria in drinking water. *Journal of microbiological Methods* **1999**, *37* (1), 77-86.
- 8 66. Zheng, S.; Bawazir, M.; Dhall, A.; Kim, H.-E.; He, L.; Heo, J.; Hwang, G.,  
9 Implication of surface properties, bacterial motility, and hydrodynamic conditions on bacterial  
10 surface sensing and their initial adhesion. *Frontiers in Bioengineering and Biotechnology* **2021**,  
11 *9*, 82.
- 12 67. Müller, P.; Saúl, A., Elastic effects on surface physics. *Surface Science Reports* **2004**, *54*  
13 (5-8), 157-258.
- 14 68. Liu, T.; Cui, Q.; Wu, Q.; Li, X.; Song, K.; Ge, D.; Guan, S., Mechanism study of  
15 bacteria killed on nanostructures. *The Journal of Physical Chemistry B* **2019**, *123* (41), 8686-  
16 8696.
- 17 69. Bauchau, O. A.; Craig, J. I., Euler-Bernoulli beam theory. In *Structural analysis*,  
18 Springer: 2009; pp 173-221.
- 19 70. Enright, M. C.; Robinson, D. A.; Randle, G.; Feil, E. J.; Grundmann, H.; Spratt, B. G.,  
20 The evolutionary history of methicillin-resistant *Staphylococcus aureus* (MRSA). *Proceedings of*  
21 *the National Academy of Sciences* **2002**, *99* (11), 7687-7692.
- 22 71. Cornelissen, C. N.; Harvey, R. A.; Fisher, B. D., *Microbiology*. Lippincott Williams &  
23 Wilkins: 2012; Vol. 3.
- 24 72. Otto, M., Staphylococcal Biofilms. *Current topics in microbiology and immunology*  
25 **2008**, 322.
- 26 73. Furukawa, S.; Akiyoshi, Y.; Komoriya, M.; Ogihara, H.; Morinaga, Y., Removing  
27 *Staphylococcus aureus* and *Escherichia coli* biofilms on stainless steel by cleaning-in-place (CIP)  
28 cleaning agents. *Food Control* **2010**, *21* (5), 669-672.
- 29 74. Duanis-Assaf, T.; Reches, M., Factors influencing initial bacterial adhesion to antifouling  
30 surfaces studied by single-cell force spectroscopy. *iScience* **2024**, *27* (2), 108803.
- 31 75. Heilmann, C., Adhesion Mechanisms of Staphylococci. *Bacterial Adhesion: Chemistry,*  
32 *Biology and Physics*, Linke, D.; Goldman, A., Eds. Springer Netherlands: Dordrecht, 2011; pp  
33 105-123.
- 34 76. WM, D., Bacterial adhesion: seen any good biofilms lately?. *Clinical microbiology*  
35 *reviews* **2002**, *15* (2), 155-166.
- 36 77. Rebane, I.; Priks, H.; Levin, K. J.; Sarigül, İ.; Mäeorg, U.; Johanson, U.; Piirimägi,  
37 P.; Tenson, T.; Tamm, T., Microbial growth and adhesion of *Escherichia coli* in elastomeric  
38 silicone foams with commonly used additives. *Scientific Reports* **2023**, *13* (1), 8541.
- 39 78. Craft, K. M.; Nguyen, J. M.; Berg, L. J.; Townsend, S. D. Methicillin-Resistant  
40 *Staphylococcus aureus* (MRSA): Antibiotic Resistance and the Biofilm Phenotype.  
41 *MedChemComm* **2019**, *10* (8), 1231-1241.
- 42 79. Maikranz, E.; Spengler, C.; Thewes, N.; Thewes, A.; Nolle, F.; Jung, P.; Bischoff, M.;  
43 Santen, L.; Jacobs, K. Different Binding Mechanisms of *Staphylococcus aureus* to Hydrophobic  
44 and Hydrophilic Surfaces. *Nanoscale* **2020**, *12* (37), 19267-19275.
- 45 80. Pratt, L. A.; Kolter, R., Genetic analysis of *Escherichia coli* biofilm formation: roles of  
46 flagella, motility, chemotaxis and type I pili. *Molecular Microbiology* **1998**, *30* (2), 285-293.



- 1 81. Choi, G.; Song, Y.; Lim, H.; Lee, S. H.; Lee, H. K.; Lee, E.; Choi, B. G.; Lee, J. J.;  
2 Im, S. G.; Lee, K. G., Antibacterial nanopillar array for an implantable intraocular lens.  
3 *Advanced Healthcare Materials* **2020**, *9* (18), 2000447.
- 4 82. Kang, S. H.; Pokroy, B.; Mahadevan, L.; Aizenberg, J., Control of shape and size of  
5 nanopillar assembly by adhesion-mediated elastocapillary interaction. *Acs Nano* **2010**, *4* (11),  
6 6323-6331.

7



## Data Availability Statements

Raw data for this article, including stiffness, swelling, micrographs, are available at [10.57760/sciencedb.36367](https://doi.org/10.57760/sciencedb.36367).

